THE JOURNAL OF PHYSICAL CHEMISTRY B

ARTICLE

pubs.acs.org/JPCB

Responsive Behaviors of Diblock Polyampholyte Brushes within Self-Consistent Field Theory

Li-Jian Qu,[†] Xingkun Man,[†] Charles C. Han,[†] Dong Qiu,*[,†] and Dadong Yan*[,‡]

[†]Beijing National Laboratory for Molecular Sciences, Joint Laboratory of Polymer Science and Materials, Institute of Chemistry, Chinese Academy of Sciences, Beijing 100190, China

[‡]Department of Physics, Beijing Normal University, Beijing 100875

ABSTRACT: Self-consistent field theory (SCFT) calculation has been performed to study the structure and stimuli-responsive behaviors of diblock polyampholyte (PA) brushes. Two kinds of brushes are considered: one formed by PA chains consisting of two strong polyelectrolyte blocks (system *i*) and the other formed by PA chains of a grafted strong acid block and an ungrafted weak base block (system *ii*). Density profiles and brush thickness are obtained. The chain trajectory (average position of each polymer segment) is also calculated to characterize the conformation of the grafted chains. For system *i*, the ungrafted blocks loop backward at low salt concentration and extend out at high salt concentration. For system *ii*, the charge fraction of the annealing block is independent of pH and becomes dependent on it at high salt concentration. As a result, pH has no effect on the brush structure at low salt concentration and takes effect at high salt concentration. That the salt concentration can switch on and off the responses of the PA brush to the pH stimuli may find application in building functional surfaces.

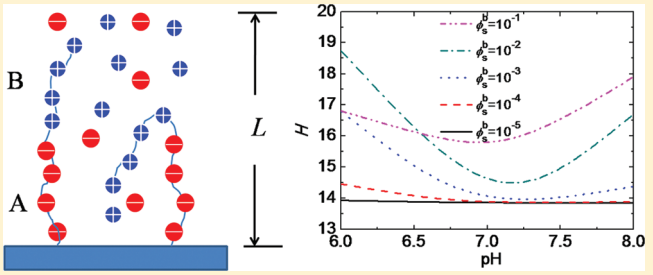

1. INTRODUCTION

Polymer brushes are made of polymer chains grafted onto a surface by covalent bonding or physical adsorption so densely that they are stretched away from the surface in a brush-like conformation. The polymer brushes which are composed of ionizable polymer (polyelectrolyte) chains are also called polyelectrolyte brushes. These systems have been studied intensively by theories,[1−8] simulations,[9−13] and experiments[14−20] due to their wide application in colloidal stabilization,[21] lubrication,[22−24] surface protection,[25] etc. Most of the progress has been summarized in reviews.[26,27]

Previous studies were mainly concerned with homopolyelectrolyte brushes, charged monomers of which are of the same sign. There is another important kind of polyelectrolyte carrying charged monomers of both signs, which is called polyampholyte (PA). Significant progress has been made in free polyampholyte chains in solution, as summarized in reviews.[28−31] A remarkable characteristic of polyampholyte chains is to respond to many controllable factors. The properties of free polyampholyte chains are dependent on the sequence of and relative fraction of positively and negatively charged segments. Charge distribution on a polyampholyte chain can be adjusted during synthesis and by solution pH if the ionizable segments are weak acids or bases. Block polyampholytes can form micelles in solutions. Polyampholyte behavior can also be tuned by adding salts into its solution.

Polyampholyte chains are also able to be used to form polymer brushes. Polyampholyte brush has been realized by many experiments. Huck et al. synthesized the triblock polyampholyte brush composed of cationic, neutral, and anionic segments.[32] The P2VP-*b*-PAA brushes were synthesized by Yu et al.[33] These authors revealed that the brush's wetting behavior could be tuned with pH. Brittain's group[34,35] investigated stimuli-responsive properties of synthesized polyampholyte brushes of poly(acrylic acid-*b*-vinyl pyridine).

Besides experimental studies, there have also been many theoretical and simulation studies. P. Linse's research group[36,37] applied lattice mean field theory to diblock polyampholyte brushes. They also studied spherical brushes of diblock polyampholytes[38,39] using the lattice mean field theory and Monte Carlo simulation method. Baratlo and Fazli[40] studied the effects of sequences of charged monomers on the planar semiflexible polyampholyte using molecular dynamics simulation. These authors studied the effects of chain stiffness of planar diblock polyampholyte brush in their following paper,[41] in which a scaling analysis was presented to flexible brushes.

As indicated in the previous studies, the conformations of the grafted PA chains respond differently to different stimuli, such as pH, salt concentration, temperature, etc. Different conformations mean different surface properties, so the PA brush has a potential for building tunable functional surfaces. In the present paper, we will theoretically investigate the responsive behavior of planar diblock polyampholyte brushes. Two kinds of polyampholyte brushes are investigated. In the first system, the

Received: October 23, 2011
Revised: December 8, 2011
Published: December 14, 2011

ACS Publications © 2011 American Chemical Society

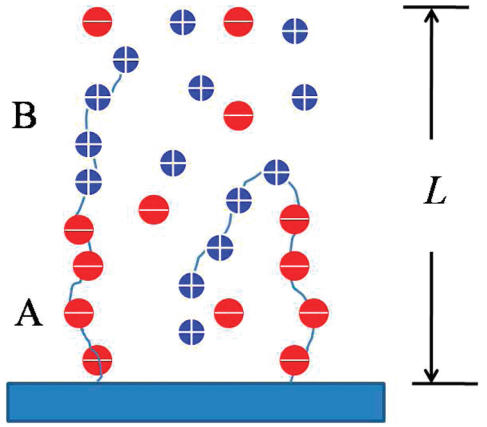

Figure 1. Schematic illustration of a polyampholyte brush. For the sake of clarity, the charges on the grafted polyampholyte chains are illustrated in a discretized manner, although the continuous distribution of charge is adopted in the SCF calculations.

polyampholyte chain is composed of two quenchedly oppositely charged blocks. For the polyampholyte chain in the second system, the block grafted to wall is quenchedly charged while the second block is annealedly charged. Salt and pH response of polyampholyte brushes are studied from theoretical calculations.

The continuous self-consistent field theory (SCFT) is used in the present study. The continuous SCFT is a powerful theoretical tool in polymer physics and has been applied to study many polyelectrolyte systems, for example, inhomogeneous polyelectrolyte solutions,[42,43] adsorption of polyelectrolytes,[44−46] polyelectrolyte confinement,[47] mixed polyelectrolyte brushes,[48] and annealed polyelectrolyte brushes.[8]

2. MODEL AND THE THEORETICAL FRAMEWORK

The studied system is schematically presented in the cartoon, Figure 1. There are n_p polyampholyte chains of length N grafted onto an uncharged planar surface. The chains are grafted uniformly with the grafting density σ chains per unit area. The system is assumed to be invariant with the directions parallel to the grafting surface, so we can only consider the evolution of physical quantities along the direction perpendicular to the surface (denoted by z). The system at $z = L$ contacts the bulk salt solution of concentration ϕ_s^b. The numbers of cations and anions are n_+ and n_-, respectively. The polyampholyte chains are composed of two blocks: block A grafted to the surface and an ungrafted block B, with the corresponding lengths N_A and N_B, respectively. Block A is negatively charged with smeared charge fraction f_A. Two different kinds of block B are considered: (*i*) positively charged with smeared charge fraction f_B (strong polyelectrolyte) and (*ii*) positively charged with a charge fraction $f_B(z)$ dependent on the local concentration of hydroxide (OH^-) ions (weak polyelectrolyte). Species in the system are denoted as P (polymer segment), A (grafted block segment), B (ungrafted block segment), + (cation), − (anion), S (solvent).

As the SCFT for polyelectrolyte systems has been well documented, here we only give the main SCF equations below. You may refer to refs 42 and 43 for the derivation details. The mean field equations are obtained from minimization of the free energy functional of the system, which, in units of k_BT, is given by

$$\begin{aligned}\frac{F}{\rho_0} = \int dz\{&\chi_{AS}\phi_A(z)\phi_S(z) + \chi_{BS}\phi_B(z)\phi_S(z)\\ &+ \chi_{AB}\phi_A(z)\phi_B(z) + [\nu_+\phi_+(z) + \nu_-\phi_-(z)]\psi(z)\\ &- \frac{1}{8\pi\rho_0 l_B}|\nabla\psi(z)|^2 + \phi_S(z)\ln([\phi_S(z)] - 1)\\ &- \omega_A(z)\phi_A(z) - \omega_B(z)\phi_B(z) - \omega_+(z)\phi_+(z)\\ &- \omega_-(z)\phi_-(z)\} - \frac{n_+}{\rho_0}\ln Q_+ - \frac{n_-}{\rho_0}\ln Q_- - \frac{n_P}{\rho_0}\ln Q_P\end{aligned} \tag{1}$$

Now we explain the meanings of the symbols in the free energy functional. $\phi_j(z)$ and $\omega_j(z)$ denote the volume fraction and the auxiliary field of species j, with j = P, A, B, S, +, and −. χ_{ij} is the Flory−Huggins parameter between species i and j. $\psi(z)$ is the electrostatic potential in units of k_BT/e, where e is the charge of a proton, k_B is the Boltzmann constant, and T is the absolute temperature. The Bjerrum length of the system is $l_B = e^2/(4\pi\varepsilon k_BT)$, where ε is the dielectric constant and assumed to be uniform. The two blocks have the same Kuhn length b. We assume that the solvent molecule and the polymer segment are of the same size, with the volume $b^3 = 1/\rho_0$. The valence of A segments, B segments, cations, and anions are ν_A, ν_B, ν_+, and ν_-, respectively. $Q_\pm$ and Q_P are the partition function for small ions and polymer chains, respectively, which follow the equations below

$$Q_\pm = \int dz\, \exp[-\omega_\pm(z)] \tag{2}$$

$$Q_P = \frac{\int \mathcal{D}z(s)\, \exp\left\{-\int_0^N ds\left[\frac{3}{2b^2}\left(\frac{\partial z(s)}{\partial s}\right)^2\right] + \omega_P[z(s)] + g_P[z(s)]\right\}}{\int \mathcal{D}z(s)\, \exp\left\{-\int_0^N ds\frac{3}{2b^2}\left(\frac{\partial z(s)}{\partial s}\right)^2\right\}} \tag{3}$$

where $g_P[z(s)]$ originates from the charge distribution along the polymer chains. The readers may refer to ref 43 for details. Since the grafted block always has a smeared charge distribution, we have $g_A(z) = \nu_A f_A \psi(z)$. Two cases for the ungrafted block are considered: for the smeared case, $g_B(z) = \nu_B f_B \psi(z)$, while, for the annealed case, $g_B(z) = -\ln[1 - f_B^b \exp(-\nu_B\psi(z))]$. When the ungrafted block is weak polyelectrolyte (in weak base case), the position dependent charge fraction:

$$f_B(z) = \frac{K_b}{K_b + [OH^-]\exp[\psi(z)]} \tag{4}$$

where K_b is the base equilibrium constant. In bulk solution, $f_B^b = K_b/(K_b + [OH^-])$. This relation is similar to weak polyacid.[5,8]

Taking $\delta F/\delta\phi_j(z) = 0$, $\delta F/\delta\omega_j(z) = 0$, and $\delta F/\delta\psi(z) = 0$, we can obtain the self-consistent field (SCF) equations

$$\begin{aligned}\omega_A(z) = &-\ln[1 - \phi_A(z) - \phi_B(z)]\\ &+ \chi_{AS}[1 - 2\phi_A(z) - \phi_B(z)]\\ &+ (\chi_{AB} - \chi_{BS})\phi_B(z)\end{aligned} \tag{5}$$

dx.doi.org/10.1021/jp210165t |*J. Phys. Chem. B* 2012, 116, 743–750

$$\omega_B(z) = -\ln[1-\phi_A(z)-\phi_B(z)] + \chi_{BS}[1-2\phi_B(z)-\phi_A(z)] + (\chi_{AB}-\chi_{AS})\phi_A(z) \quad (6)$$

$$\omega_\pm(z) = \nu_\pm\psi(z) \quad (7)$$

$$\phi_A(z) = \frac{\sigma}{\rho_0 Q_P}\int_0^{N_A} ds q(z,s)q\dagger(z,N-s) \quad (8)$$

$$\phi_B(z) = \frac{\sigma}{\rho_0 Q_P}\int_{N-N_B}^{N} ds q(z,s)q\dagger(z,N-s) \quad (9)$$

$$Q_P = \int_0^L dz q(z,N) \quad (10)$$

$$\phi_\pm(z) = \phi_\pm^b \exp[-\omega_\pm(z)] \quad (11)$$

$$\frac{d^2\psi(z)}{dz^2} = -4\pi l_B[\nu_A f_A\phi_A(z) + \nu_B f_B(z)\phi_B(z) + \nu_+\phi_+(z) + \nu_-\phi_-(z)] \quad (12)$$

In the equations above, $s \in [0,N]$ is the variable along the chain tour. $q(z,s)$ denotes the statistical weight of a subchain starting at the grafting surface and ending at z in s steps, and $q\dagger(z,s)$ is the end-monomer distribution function of a subchain starting anywhere except the grafting surface and terminating at z in s steps. They each satisfy the following modified diffusion equations, respectively:

$$\frac{\partial q(z,s)}{\partial s} = \frac{b^2}{6}\frac{\partial^2}{\partial z^2}q(z,s) - [\omega_P(z) + g_P(z)]q(z,s) \quad (13)$$

and

$$\frac{\partial q\dagger(z,s)}{\partial s} = \frac{b^2}{6}\frac{\partial^2}{\partial z^2}q\dagger(z,s) - [\omega_P(z) + g_P(z)]q\dagger(z,s) \quad (14)$$

where $\omega_P(z) = \omega_A(z)$ for $s \le N_A$ and $\omega_P(z) = \omega_B(z)$ for $N - N_B \le s \le N$.

Finally, the system is assumed to be incompressible and small ions are taken to be point charges without excluded volume; thus,

$$\phi_P(z) + \phi_S(z) = 1 \quad (15)$$

Previous SCFT calculations on polyelectrolyte brushes[8] have indicated that the ion volume has only minimal effects and does not affect the general trend. Therefore, here we do not consider the ion volume, although the ion volume can be easily incorporated in our theory.

To solve the modified diffusion equations of eqs 13 and 14 and the Poisson−Boltzmann equation of eq 12, proper boundary and initial conditions are required. We adopt the boundary conditions as $d\psi(z)/dz|_{z=0} = 0$, $d\psi(z)/dz|_{z=L} = 0$, $q(z=0, s>0) = 0$, $q\dagger(z=0, s<N) = 0$, $q\dagger(z=0, s=N) = 1$, $q(z=L, s) = 0$, and $q\dagger(z=L,s) = 0$ and the initial conditions as $q(z=0,s=0) = 1$, $q(z>0, s=0) = 0$, and $q\dagger(z>0, s=0) = 1$. The boundary conditions imply that the grafting surface is impenetrable for the grafted chains and the grafted chains cannot extend outside the upper boundary $z = L$.

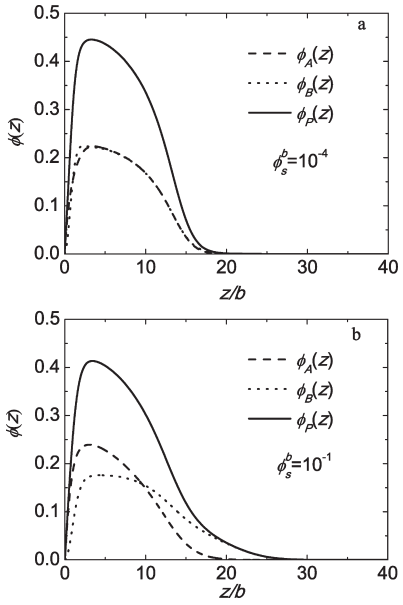

Figure 2. Density profiles of both blocks (A and B) and their sum: (a) $\phi_s^b = 10^{-4}$, (b) $\phi_s^b = 10^{-1}$. The charge fractions of blocks A and B are fixed, $f_A = f_B = 0.5$.

The SCF equations 5−14 are solved numerically in real space following ref 44. The set of nonlinear equations are solved using Broyden's method,[49] and the modified diffusion equations 13 and 14 are solved using the Crank−Nicolson scheme.[49]

3. RESULTS AND DISCUSSION

The numerical results of the SCFT on the polyampholyte brushes will be given in this section. In our calculations, the parameters are taken as follows if not specified. The monomer length $b = 0.5$ nm, which is used as the length unit throughout the paper. $l_B = 0.7$ nm for water at room temperature. 1:1 electrolytes are used as added salt and the charged monomers are monovalently charged, so $\nu_+ = -\nu_- = -\nu_A = \nu_B = 1$ and $\phi_\pm^b = \phi_s^b$. We take $\chi_{AS} = \chi_{BS} = 0.5$ and $\chi_{AB} = 0$; that is, the solvent is θ for both blocks and the two blocks are chemically the same except the charge they bear. The grafting density is fixed at $\sigma = 0.05b^{-2}$. The chain length is $N = 100$ and the lengths of the two blocks are equal to each other, $N_A = N_B = N/2$. We select $L = Nb$, which is wide enough not to influence the chain statistics and reaches the bulk solution. The grafted block bears negative charges and the ungrafted block bears positive charges of quenched (quenched PA brush) or annealed (semiannealed PA brush) distribution.

3.1. Quenched PA Brush in Response to Salt. In this section, we study the quenched PA brushes formed by PA chains consisting of two strong polyelectrolyte blocks. The charge fractions of blocks A and B are fixed at $f_A = f_B = 0.5$, which applies to all the results in this section.

Figure 2 shows the segmental profiles of the PA brush at low and high salt concentrations of $\phi_s^b = 10^{-4}$ (Figure 2a) and 10^{-1} (Figure 2b). Similar calculations have been conducted using lattice SCF.[36,37] The results of the continuous and lattice SCF calculations are similar to each other because the essence of both methods are the same. Both continuous and lattice SCF calculations show that there is a depletion layer near the grafting surface because of its impenetrability. Similar density profiles are obtained by continuous and lattice SCF calculations. The profiles

dx.doi.org/10.1021/jp210165t |J. Phys. Chem. B 2012, 116, 743–750

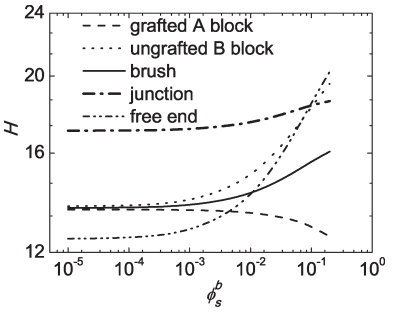

Figure 3. Dependence of thickness of the two blocks, the brush, the junctions, and the free ends on salt concentration in double logarithm coordinates.

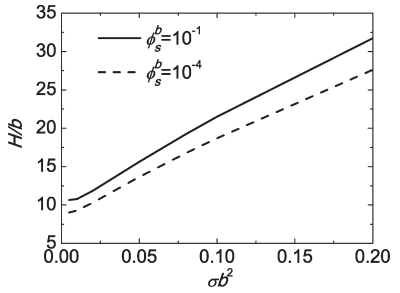

Figure 4. Dependence of the thickness of PA brush on the grafting density at high ($\phi_s^b = 10^{-1}$) and low ($\phi_s^b = 10^{-4}$) salt concentration.

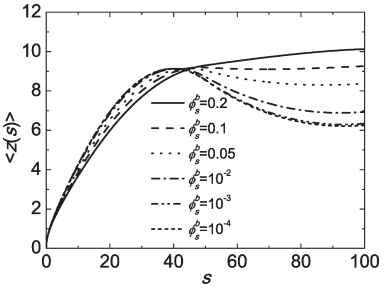

Figure 5. Average trajectories for PA brushes with various salt concentrations.

are the first step for latter discussion, so we still represent and discuss these results here.

As seen in Figure 2, the profiles of A and B segments at low salt concentrations almost overlap with each other and have only minor differences near the grafting wall and the brush brim. With the increase of the salt concentration, the profiles of A and B segments gradually separate apart. When the salt concentration is low, the electrostatic attraction between A and B segments makes the last block fold back toward the grafted block. They completely compensate each other so their density profiles show almost identical behavior. At high salt concentrations, or $\phi_s^b = 0.1$, the density profiles of the two blocks evidently separate from each other. The density profile of the grafted block changes little and that of the ungrafted block extends outward with the increase of the salt concentration. This is due to the reason that the electrostatic interaction between A and B blocks is partially screened by the added salt and hence the ungrafted block detaches from the grafted block in some extent. At any salt concentration, the total density profiles of the brush follow a parabola-like curve, which is a typical behavior of the neutral brush. This is an expected result, since the brush is almost locally electroneutral under any conditions.

Figure 3 represents the effect of salt concentration on the thickness of the grafted and ungrafted block, the brush, the free ends, and the junctions. The free end is the last segment, and the junction is the connecting point of the A and B blocks. The brush thickness is defined as

$$H = 2\frac{\int_0^\infty z\phi_P(z)\ dz}{\int_0^\infty \phi_P(z)\ dz} \tag{16}$$

where $\phi_P(z) = \phi_A(z) + \phi_B(z)$. Other thicknesses can be defined similarly.

For homopolyelectrolyte brush, the electrostatic interactions between polymer segments are screened by the added salt, so the brush height decreases with the increase of the salt concentration. For diblock polyampholyte brush, the ungrafted block loops backward to the grafted block driven by electrostatic attraction. When a significant amount of salt is added into the brush, the electrostatic attraction is screened by the salt, so some of the looped ungrafted block will stretch outward. In Figure 3, the thickness of ungrafted block and free ends increases with the salt concentration, which is consistent with the picture above. The thickness of the grafted block decreases with the salt concentration, similar to the behavior of homopolyelectrolyte brush. The increase of the thickness of the ungrafted block is more significant than the decrease of the height of the grafted block, so the overall brush height increases with the salt concentration. The thickness of the junction depends inconspicuously on the salt concentration, because the grafted and ungrafted blocks balance at the junction.

Figure 4 shows the brush thickness as a function of grafting density at high ($\phi_s^b = 10^{-1}$) and low ($\phi_s^b = 10^{-4}$) salt concentrations. The brush thickness demonstrates a good linear relationship with the grafting density, $H \sim \sigma$, at both high and low salt concentrations. The proportional relation between the thickness of PA brush without salt and the grafting density has been observed in computer simulation.[41] The SCF calculations indicate that the brush thickness is still proportional to the grafting density when salt is added to the solution. The brush thickness at high salt concentration is higher than that at low salt concentration, which is consistent with Figure 3.

To characterize the chain behavior details, we give chain trajectories of the grafted PA chains in Figure 5. The chain trajectory is defined as the average location of any segment

$$\langle z(s)\rangle = \frac{\int_0^\infty zq(z,s)q\dagger(z,s)\ dz}{\int_0^\infty q(z,s)q\dagger(z,s)\ dz} \tag{17}$$

From Figure 5, we can see that the salt concentration has little effect on the brush when it is lower than $\phi_s^b = 10^{-3}$. The average location of ungrafted block, $\langle z(s > 50)\rangle$, is clearly smaller than that of the AB-junction, $\langle z(s = 50)\rangle$, at low salt concentrations. It indicates that the ungrafted blocks loop back toward the grafting wall. As the salt concentration increases, more and more

dx.doi.org/10.1021/jp210165t |J. Phys. Chem. B 2012, 116, 743–750

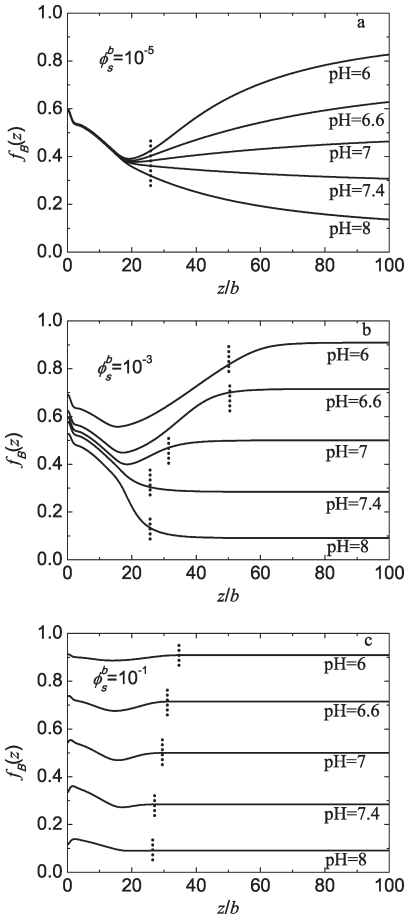

Figure 6. Charge fraction of the ungrafted block as a function of distance to the grafting surface at $\phi_s^b = 10^{-5}$ (a), $\phi_s^b = 10^{-3}$ (b), and $\phi_s^b = 10^{-1}$ (c). The dotted lines on the curves denote the maximum distance the brushes extend.

small ions come into the brush region to screen the electrostatic interaction between the two oppositely charged blocks, so the average location of the B block increases. At salt concentration $\phi_s^b = 0.1$, the curve of the average position of the ungrafted block levels off. At even higher salt concentration, $\phi_s^b = 0.2$, the average location of the whole chain increases consistently with the segment number. The trajectories indicate that the grafted blocks contract with the increase of the salt concentration, which is consistent with the behavior of brush thickness, as shown in Figure 3. The slight contraction of the grafted blocks with the increase of the salt concentration can also be observed from $\langle z(s < 50)\rangle$ in Figure 5. The two blocks balance at the segment near the junction, which is the intersection point of the trajectories.

From polymer segment density profiles and the chain trajectory shown above, we may conjecture the brush responsive behavior to the added salt as follows. At low salt concentration, the ungrafted blocks loop backward and form polyelectrolyte complexes with the oppositely charged grafted blocks driven by electrostatic attraction. At intermediate salt concentrations, some looped ungrafted blocks stretch out as the electrostatic attraction is weakened by the salt screening. However, polyelectrolyte complexes still exist in the brush as the electrostatic attraction between the oppositely charged blocks is still strong enough. Under these conditions, the chain trajectory presents a plateau,

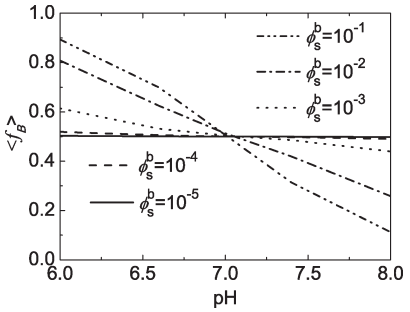

Figure 7. Average charge fraction of the ungrafted B-block as a function of pH.

as shown in Figure 5. Going on increasing salt concentrations, the remaining polyelectrolyte complexes will disassemble and almost all of the polymer chains on average stretch outward. This case is manifested in the chain trajectory at salt concentration $\phi_s^b = 0.2$ in Figure 5.

3.2. Semiannealed PA Brush in Response to pH. The results above are valid for strong polyampholyte brush. In this section, we will explore the weak polyelectrolyte cases, where the charge fraction of the polyelectrolyte chains can be tuned easily by the pH of the solution. In our study, the grafted block is still strong polyelectrolyte bearing negative charges as in the above sections, while the ungrafted block is a weak polyalkali, that is, a semiannealed PA brush. The base equilibrium constant $K_b = 10^{-7}$ is selected. We mainly focus on the responsive behavior of the ungrafted block to pH at different salt concentrations.

In Figure 6, we plot the charge fraction $f_B(z)$, following eq 4, of the ungrafted block as a function of the distance to the grafting wall. It should be noticed that the brushes do not extend all over the region in Figure 6. Physically, the brush extends to a finite distance. The region inside this distance is called the brush region. The brush region is marked with a dotted line in Figure 6, which is estimated with $\phi_P(z) < 10^{-3}$. Now we focus on the brush region in Figure 6. At low concentration, $\phi_s^b = 10^{-5}$ in Figure 6a, all the brushes show almost the same dissociation behavior in the brush region irrespective of the pH in the bulk solution. At intermediate salt concentration, $\phi_s^b = 10^{-3}$ in Figure 6b, the $f_B(z)$ curves of different pH begin to separate but are still near each other. At high salt concentration, $\phi_s^b = 10^{-1}$ in Figure 6c, the $f_B(z)$ curves separate significantly. At any salt concentration, the charge fraction decreases monotonously from a higher value to a lower value and then reaches the bulk value, which is totally different from the weak homopolyelectrolyte brush. For weak homopolyelectrolyte brush, the charge fraction always increases from a lower value to the bulk value. The different behavior of diblock strong−weak polyelectrolyte brush is attributed to the grafted block. The grafted blocks, bearing charges of the same sign with the OH^- ions, make the OH^- concentration distribute in a contrary way with the grafted A segments, so that the charge fraction of the ungrafted block decreases with the distance from the grafting surface. At low salt concentration, the OH^- concentration is mainly controlled by the grafted block, so the charge fraction curves of the grafted block of different pH overlap with each other. The charge fraction of the ungrafted blocks is close to that of the grafted blocks, which can lower the free energy of the system though at the expense of the conformal entropy. With the salt concentration increasing, the OH^- concentration begins to be affected by the salt, so the charge fraction curves separate at

dx.doi.org/10.1021/jp210165t |J. Phys. Chem. B 2012, 116, 743–750

comparatively high salt concentration, then the grafted chains gain some conformational entropy.

Figure 7 shows the effects of pH on the average charge fraction of the ungrafted blocks at various salt concentrations. The average charge fraction is calculated according to

$$\langle f_B \rangle = \frac{\int_0^\infty f_B(z)\phi(z)\ dz}{\int_0^\infty \phi(z)\ dz} \quad (18)$$

At low salt concentrations, $\phi_s^b = 10^{-5}$, the average charge fraction, $\langle f_B \rangle$, is almost invariant with the pH, the value close to the charge fraction of the grafted block. Under higher salt concentrations, $\langle f_B \rangle$ is approximately in a linear relation to the pH. The slope of the lines increases with the increase of salt concentration, which indicates that the dissociation of the ungrafted blocks is more easily influenced by pH at high salt concentration. All the lines intersect at pH 7.

Density profiles of the brushes are given in Figure 8 under conditions of different salt concentrations and pH. At low salt concentrations of $\phi_s^b = 10^{-5}$ (Figure 8a and d), the density profiles are independent of pH and show almost the same behavior. The two blocks overlap each other like strong PA brushes, as shown in Figure 2a. This is an expected result as the ungrafted blocks show almost the same charge dissociation behavior with a mean charge fraction close to that of the grafted blocks. At an intermediate salt concentration of $\phi_s^b = 10^{-3}$, the density profiles of brush of pH = 6 (Figure 8b) show a long tail, which is a typical behavior in homopolyelectrolyte brush.[7] What accounts for this homopolyelectrolyte-like behavior is that the ungrafted blocks with excess charge will extend outward because of electrostatic repulsion. The density profiles shrink significantly when the salt concentration is as high as $\phi_s^b = 0.1$ (Figure 8c), as a result of the electrostatic screening of the added salt. At pH = 8, comparing Figure 8d and e, the overlapping extent of the density profiles of both blocks weakens with the increase of salt concentration, and the two blocks' density profiles significantly separate at high salt concentration $\phi_s^b = 0.1$, as shown in Figure 8f.

These behaviors are the results of electrostatic screening and the decrease of the charge fraction of the ungrafted block.

The brush thickness as a function of pH at various salt concentrations is shown in Figure 9. At low salt concentration ($\phi_s^b = 10^{-5}$ and 10^{-4}), the brush thickness is almost invariant with the pH, which is consistent with the invariance of the charge fraction of the ungrafted blocks $f_B(z)$ with the pH at such salt concentrations, as shown in Figures 6 and 7. The curves resemble a chair at intermediate salt concentrations ($\phi_s^b = 10^{-3}$). The insignificant dependence of the thickness on the pH for pH > 7 is because of no significant difference between the charge of the two blocks. The pH dependence of brush thickness at salt concentrations of $\phi_s^b > 10^{-3}$ shows two obvious monotonous zones. When pH < 7, the charge fraction of the ungrafted block is larger than that of the grafted block, and the excess charge decreases with the increase of the pH, and so is the brush thickness. When pH > 7, the ungrafted blocks bear less charge than the grafted blocks do. The less charging of the ungrafted blocks with the increase of salt concentration and the electrostatic screening account for the brush thickness's increase with the pH when pH > 7.

The chain conformation response to pH is shown in Figure 10. At a low salt concentration of $\phi_s^b = 10^{-5}$ (Figure 10a), the ungrafted blocks loop back and form complexes, almost unaffected by the pH. This behavior is consistent with the dissociation behavior of the ungrafted block (as shown in Figures 6 and 7).

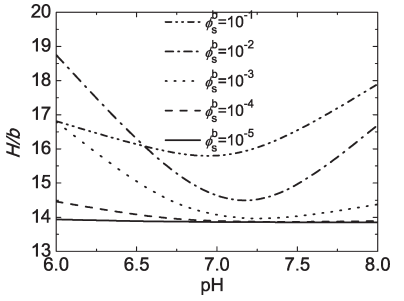

Figure 9. Dependence of PA brush thickness on the pH at various salt concentrations.

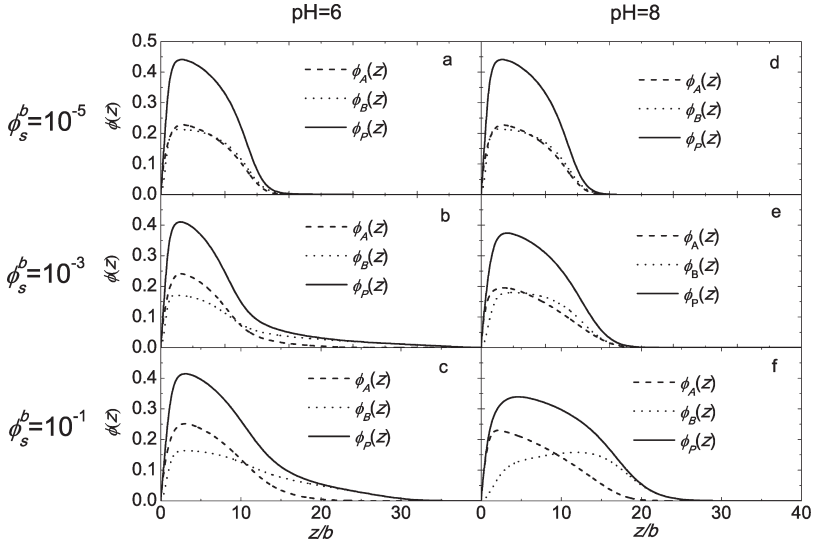

Figure 8. Effects of pH on density profiles of both blocks (A and B) and their sum at three salt concentrations: a ($\phi_s^b = 10^{-5}$), b ($\phi_s^b = 10^{-3}$), and c ($\phi_s^b = 10^{-1}$) for pH 6; d ($\phi_s^b = 10^{-5}$), e ($\phi_s^b = 10^{-3}$), and f ($\phi_s^b = 10^{-1}$) for pH 8. $f_A = 0.5$ in all the figures.

dx.doi.org/10.1021/jp210165t | J. Phys. Chem. B 2012, 116, 743–750

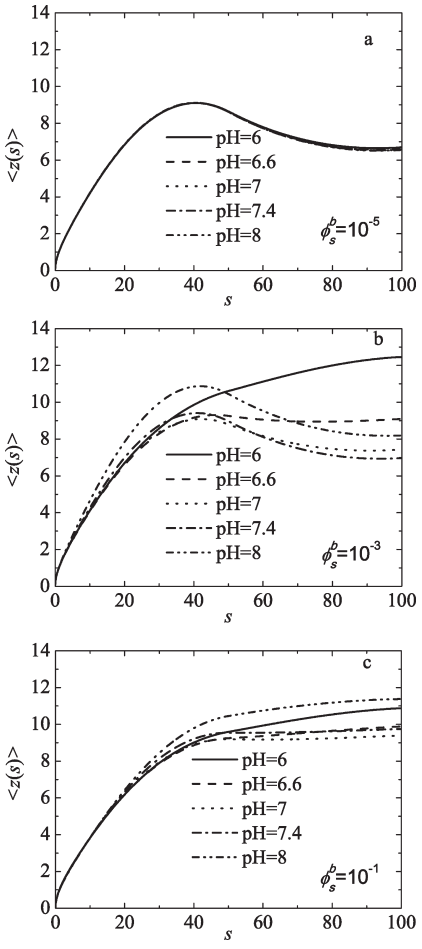

Figure 10. Effects of pH on average trajectories for PA brushes at three salt concentrations: (a) $\phi_s^b = 10^{-5}$, (b) $\phi_s^b = 10^{-3}$, and (c) $\phi_s^b = 10^{-1}$.

At an intermediate salt concentration of $\phi_s^b = 10^{-3}$ (Figure 10b), the ungrafted blocks extend outward on average at pH = 6, while the ungrafted blocks still loop back at pH > 7. This is because the ungrafted blocks bear more charges than the grafted blocks at pH = 6, while they bear less at pH > 7. The looping extent at pH = 8 is obviously less than that at pH = 7 and 7.4. The added salt lessens the looping extent by screening the electrostatic interaction, since the ungrafted blocks for pH = 8 bear less charge than those at pH = 7 and 7.4. At a high salt concentration of $\phi_s^b = 10^{-1}$ (Figure 10c), a plateau appears when the charge of the ungrafted block is near that of the grafted block (pH = 6.6, 7, 7.4). While the charge of both blocks deviates greatly, pH 6 and pH 8, the ungrafted blocks extend significantly. For pH < 7 cases, $\langle f_B \rangle > f_A$, the larger $\langle f_B \rangle$ (the smaller pH) is, the more added salt is needed to screen the excess charge, and so the ungrafted blocks under lower pH are more stretched. For the pH > 7 cases, $\langle f_B \rangle < f_A$, the added salt disassembles the complexes formed by the two polyelectrolyte blocks more easily for higher pH, and so the ungrafted blocks in solution with higher pH are more stretched.

From the results above in this part, we can find that at low salt concentration the semiannealed PA brush behaves like an inert surface, showing almost no response to pH. On the other hand, at high salt concentration, the PA brush becomes responsive to pH. These phenomena may bring applications in surface modification, controlled release, etc.

4. CONCLUSION

In this paper, we study the responsive behaviors of polyampholyte (PA) brushes to salt concentrations and pH within SCFT. The grafted diblock PA chain is composed of a negatively charged A block and a positively charged B block. The diblock PA chains are grafted onto a planar surface with A blocks. Two kinds of PA brushes have been investigated: one with two blocks of strong polyelectrolytes (system *i*: quenched PA brush) and the other with the grafted block of strong polyelectrolyte and the ungrafted block of weak polyelectrolyte (system *ii*: semiannealed PA brush).

For system *i*, the ungrafted blocks loop backward and form complexes with the oppositely charged grafted blocks because of electrostatic attraction between the two blocks. The complexes begin to disassemble with the increase of salt concentration for the more and more significant electrostatic screening.

For system *ii*, the ungrafted blocks of the PA brushes show no response to pH variation at low salt concentration. The brushes behave as brushes of PA chains without net charge in system *i*. pH takes effect when the salt concentration is high. Then you can tune the brush behaviors by varying the pH value. This inert-responsive transition may be used to build functional surface.

At the present stage, we only study the responsive behaviors of polyampholyte brushes to the added salt and pH variation. However, other stimuli can also be studied in the general model in section 2. For example, the solvent and temperature response of the PA brush can be studied by varying the Flory−Huggins parameters between different components.

AUTHOR INFORMATION

Corresponding Author

*E-mail: dqiu@iccas.ac.cn (D.Q.); yandd@bnu.edu.cn (D.Y.).

ACKNOWLEDGMENT

The authors acknowledge the financial support of National Natural Science Foundation of China (NSFC) 20990234, 208 74111, 20973176, 508211062, 973 Program of the Ministry of Science and Technology (MOST) 2011CB808502, and the Fundamental Research Funds for the Central Universities.

REFERENCES

(1) Pincus, P. *Macromolecules* **1991**, *24*, 2912–2919.
(2) Zhulina, E. B.; Birshtein, T. M.; Borisov, O. V. *Macromolecules* **1995**, *28*, 1491–1499.
(3) Israels, R.; Leermakers, F. A. M.; Fleer, G. J.; Zhulina, E. B. *Macromolecules* **1994**, *27*, 3249–3261.
(4) Borisov, O. V.; Zhulina, E. B.; Birshtein, T. M. *Macromolecules* **1994**, *27*, 4795–4803.
(5) Israëls, R.; Leermakers, F. A. M.; Fleer, G. J. *Macromolecules* **1994**, *27*, 3087–3093.
(6) Zhulina, E. B.; Wolterink, J. K.; Borisov, O. V. *Macromolecules* **2000**, *33*, 4945–4953.
(7) Jiang, T.; Li, Z.; Wu, J. *Macromolecules* **2007**, *40*, 334–343.
(8) Witte, K. N.; Kim, S.; Won, Y. Y. *J. Phys. Chem. B* **2009**, *113*, 11076–11084.
(9) Csajka, F. S.; Seidel, C. *Macromolecules* **2000**, *33*, 2728–2739.
(10) Seidel, C. *Macromolecules* **2003**, *36*, 2536–2543.
(11) Kumar, N. A.; Seidel, C. *Macromolecules* **2005**, *38*, 9341–9350.
(12) Chen, L.; Merlitz, H.; He, S.; Wu, C. X.; Sommer, J. U. *Macromolecules* **2011**, *44*, 3109–3116.

(13) Hehmeyer, O. J.; Arya, G.; Panagiotopoulos, A. Z.; Szleifer, I. *J. Chem. Phys.* **2007**, *126*, 244902.
(14) Mir, Y.; Auroy, P.; Auvray, L. *Phys. Rev. Lett.* **1995**, *75*, 2863–2866.
(15) Guenoun, P.; Schalchli, A.; Sentenac, D.; Mays, J. W.; Benattar, J. J. *Phys. Rev. Lett.* **1995**, *74*, 3628–3631.
(16) Ahrens, H.; Förster, S.; Helm, C. A. *Phys. Rev. Lett.* **1998**, *81*, 4172–4175.
(17) Romet-Lemonne, G.; Daillant, J.; Guenoun, P.; Yang, J.; Mays, J. W. *Phys. Rev. Lett.* **2004**, *93*, 148301.
(18) Ahrens, H.; Förster, S.; Helm, C. A. *Macromolecules* **1997**, *30*, 8447–8452.
(19) Balastre, M.; Li, F.; Schorr, P.; Yang, J.; Mays, J. W.; Tirrell, M. V. *Macromolecules* **2002**, *35*, 9480–9486.
(20) Guo, X.; Ballauff, M. *Phys. Rev. E* **2001**, *64*, 051406.
(21) Napper, D. H. *Polymeric stabilization of colloidal dispersions*; Academic Press: London, 1983; Vol. 7.
(22) Klein, J.; Kamiyama, Y.; Yoshizawa, H.; Israelachvili, J. N.; Fredrickson, G. H.; Pincus, P.; Fetters, L. J. *Macromolecules* **1993**, *26*, 5552–5560.
(23) Pavoor, P. V.; Gearing, B. P.; Bellare, A.; Cohen, R. E. *Wear* **2004**, *256*, 1196–1207.
(24) Sokoloff, J. B. *J. Chem. Phys.* **2008**, *129*, 014901.
(25) Wittemann, A.; Haupt, B.; Ballauff, M. *Phys. Chem. Chem. Phys.* **2003**, *5*, 1671–1677.
(26) Rühe, J.; et al. *Adv. Polym. Sci.* **2004**, *165*, 79–150.
(27) Naji, A.; Seidel, C.; Netz, R. *Adv. Polym. Sci.* **2006**, 149–183.
(28) Kudaibergenov, S. *Polymer Latexes-Epoxide Resins-Polyampholytes* **1999**, 115–197.
(29) Lowe, A. B.; McCormick, C. L. *Chem. Rev.* **2002**, *102*, 4177–4190.
(30) Dobrynin, A. V.; Colby, R. H.; Rubinstein, M. *J. Polym. Sci., Part B: Polym. Phys.* **2004**, *42*, 3513–3538.
(31) Shusharina, N. P.; Rubinstein, M. In *Nanostructured Soft Matter: Experiment, Theory, Simulation and Perspectives*; Zvelindovsky, A., Ed.; Springer: 2007; pp 301−326.
(32) Osborne, V. L.; Jones, D. M.; Huck, W. T. S. *Chem. Commun.* **2002**, 1838–1839.
(33) Yu, K.; Wang, H.; Xue, L.; Han, Y. *Langmuir* **2007**, *23*, 1443–1452.
(34) Ayres, N.; Boyes, S. G.; Brittain, W. J. *Langmuir* **2007**, *23*, 182–189.
(35) Ayres, N.; Cyrus, C. D.; Brittain, W. J. *Langmuir* **2007**, *23*, 3744–3749.
(36) Shusharina, N. P.; Linse, P. *Eur. Phys. J. E* **2001**, *4*, 399–402.
(37) Shusharina, N. P.; Linse, P. *Eur. Phys. J. E* **2001**, *6*, 147–155.
(38) Akinchina, A.; Shusharina, N. P.; Linse, P. *Langmuir* **2004**, *20*, 10351–10360.
(39) Akinchina, A.; Linse, P. *Langmuir* **2007**, *23*, 1465–1472.
(40) Baratlo, M.; Fazli, H. *Eur. Phys. J. E* **2009**, *29*, 131–138.
(41) Baratlo, M.; Fazli, H. *Phys. Rev. E* **2010**, *81*, 011801.
(42) Shi, A. C.; Noolandi, J. *Macromol. Theory Simul.* **1999**, *8*, 214–229.
(43) Wang, Q.; Taniguchi, T.; Fredrickson, G. H. *J. Phys. Chem. B* **2004**, *108*, 6733–6744.
(44) Wang, Q. *Macromolecules* **2005**, *38*, 8911–8922.
(45) Man, X.; Yang, S.; Yan, D.; Shi, A. *Macromolecules* **2008**, *41*, 5451–5456.
(46) Man, X.; Yan, D. *Macromolecules* **2010**, *43*, 2582–2588.
(47) Kumar, R.; Muthukumar, M. *J. Chem. Phys.* **2008**, *128*, 184902.
(48) Witte, K. N.; Won, Y. Y. *Macromolecules* **2006**, *39*, 7757–7768.
(49) Press, W. H.; Teukolsky, S. A.; Vetterling, W. T.; Flannery, B. P. *Numerical recipes*, 3rd ed.; Cambridge University Press: 2007.